

## 3 $\mu\text{m}$ Intersubband Quantum Well Photodetector (QWIP)

Rita GUPTA, A. L. Y. WONG, S. K. HAYWOOD

*School of Engineering, University of Hull,  
Hull HU6 7RX UK.*

Received 01.03.1999

### Abstract

In recent years photodetectors operating in the mid- to far infrared region of 3-15 $\mu\text{m}$  have been designed based on electron and hole intersubband transitions in multiple quantum wells and superlattices. In general, QWIPs based on electron transitions show greater detectivity compared to the hole-based photodetectors. However, selection rules for electron intersubband transitions usually forbid the TE mode operation, associated with normal light incidence; Therefore, special coupling structures/geometries have been employed to couple light into the device.

The spectral region 3-5 $\mu\text{m}$  is of interest for a variety of applications such as environmental gas sensing, thermal imaging etc. and is not well covered by existing detectors. We have grown a QWIP operating at  $\sim 3\mu\text{m}$  with a normal incidence component which incorporates an InGaAs/GaAs asymmetric quantum well from which photo-excited carriers undergo resonant tunnelling into the AlGaAs barriers. A study of temperature-dependent dark current of this device is presented with a view to obtaining enhanced detectivity at high temperatures.

### Introduction

Photodetectors operating in the mid- to far infra-red region of 3-30  $\mu\text{m}$  have wide-ranging applications which include thermal imaging, remote gas sensing and medical imaging. These photodetectors have usually been based on the inter-band transitions in InAs, InSb and Cd(Hg)Te. However, in recent years, photodetectors based on electron and hole intersubband transitions in multiple quantum wells and superlattices have been studied widely [1,2]. These quantum well intersubband photodetectors (QWIPs) offer greater flexibility in the design of operating wavelength of the device compared to the photodetector based on the interband transition. The operating wavelength for the latter is determined by the energy gap between the valence and conduction bands and therefore can be varied only by using alloy semiconductors such as  $\text{Cd}_x\text{Hg}_{1-x}\text{Te}$ . The operating

wavelength of QWIPs, on the other hand, may be changed by using different quantum well-widths or by using different combinations of well and barrier materials. In addition, GaAs-based QWIPs offer mature GaAs growth and processing technologies leading to high uniformity and reproducibility, and, therefore to large area and low cost detector arrays. This is in contrast to the more difficult growth and fabrication processes associated with small band-gap devices needed for detection of long wavelength radiation,  $\lambda \sim 10\mu\text{m}$  ( $E_g \sim 0.1\text{eV}$ ). QWIPs based on direct gap AlGaAs/GaAs multiple quantum wells usually have intersubband transition energies of  $\lambda \sim 10\text{-}30\mu\text{m}$ . However, recently, a InGaAs/AlAs QWIP operating at a shorter wavelength of  $3\mu\text{m}$  has been demonstrated.[3]

Intersubband photodetectors have been designed based on both transitions in the valence as well as conduction band. In general, QWIPs based on electron transitions show greater detectivity compared to the hole-based photodetectors. One of the reasons for this advantage is their lighter effective mass. However, normal selection rules for electron intersubband transitions forbid the TE mode operation, associated with the detection of light incident normal to the device surface [1]. In this case special coupling structures/geometries have been employed to couple light into the device. QWIPs based on hole transitions, on the other hand, allow detection of both TE and TM component of the incident radiation. Recently, Liu et al. [4] have shown that a relaxation in the selection rules for electron inter-subband transitions is observed as the energy band gap of the quantum well decreases.

We have designed and studied an electron-based QWIP operating at  $\sim 3\mu\text{m}$  with a component of normal incidence absorption. It is based on an asymmetric InGaAs/GaAs quantum well to allow normal incidence (TE) absorption. A series of samples with different barrier heights and thicknesses have been studied to optimize the detectivity of the device. In this paper we present results on photocurrent and dark I-V measured as a function of temperature. In Section 2 we present the details of the samples studied and experimental results obtained. Section 3 contains a discussion of these results and some concluding remarks are presented in Section 4.

## Experimental

Four samples, grown by MBE, have been studied. Figure 1 shows the generic conduction band profile of our QWIPs where the layer thicknesses  $a_1=a_2=24\text{\AA}$  and  $c=300\text{\AA}$  are kept constant. Other sample parameters are summarized in the Table. All samples contain 10 periods of the resonant tunnelling asymmetric quantum well structure incorporated in an n-i-n structure. The deepest part of the quantum well (InGaAs) was n-doped with Si:  $N_D=5.10^{18}\text{ cm}^{-3}$ . Devices were processed into mesa diodes of various diameters. Some samples have metal gratings of  $3\mu\text{m}$ ,  $5\mu\text{m}$  and  $7\mu\text{m}$  to enhance normal incidence absorption.

The relevant optical transition is from the energy level in the deepest part of the quantum well,  $\text{In}_{0.22}\text{Ga}_{0.78}\text{As}$ , to a level just above the conduction band edge of the  $\text{Al}_x\text{Ga}_{1-x}\text{As}$  barriers. In this situation, the photoexcited electrons undergo resonant tunnelling through the thin AlAs barriers into the AlGaAs. These photo-electrons are

then collected with the application of a small bias across the device. Figure 2 shows the photocurrent measured from sample 1262, under illumination at normal incidence at 78K and applied bias of 0.5 volts. The interband (hh1-c1) transition at  $\sim 700-900$  nm and the intersubband transitions at 2.3-3.3  $\mu\text{m}$  are clearly seen. The two photocurrent peaks were measured using two different gratings of the monochromator and are not normalised with respect to each other. It is also not possible to compare the relative magnitudes of the two peaks due to the absorption of radiation by water vapour at  $\sim 2.7\mu\text{m}$ .

**Table A** summary of the parameters of the samples studied.

Sample	$b_1$ (Å)	$b_2$ (Å)	x
1262	40	12	0.32
1372	40	12	0.40
1373	60	20	0.40
1374	60	20	0.32

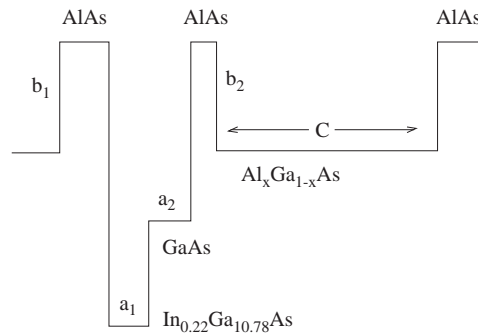


**Figure 1.** Generic conduction band profile of the QWIP structures studied. For sample parameters see the text and the Table.

Figure 3 shows the dark I-V measurements on 400  $\mu\text{m}$  diameter devices at 150K for all four samples. Samples 1262 and 1374 show significantly higher dark currents compared to 1372 and 1373. Dark current measurements for the four samples at 230K are presented in Fig. 4 and the experimental results are discussed in the next section.

### Discussion of results

The most important parameters for optimisation of the performance of IR MQW detectors are dark current, collection efficiency and correlated noise effects. [5] In our samples, the resonant tunnelling nature of the energy level to which the electrons are photo-excited to ensures a high collector efficiency. With this in mind, we chose the parameters of the four samples to obtain greater understanding of the mechanisms contributing to the dark current.

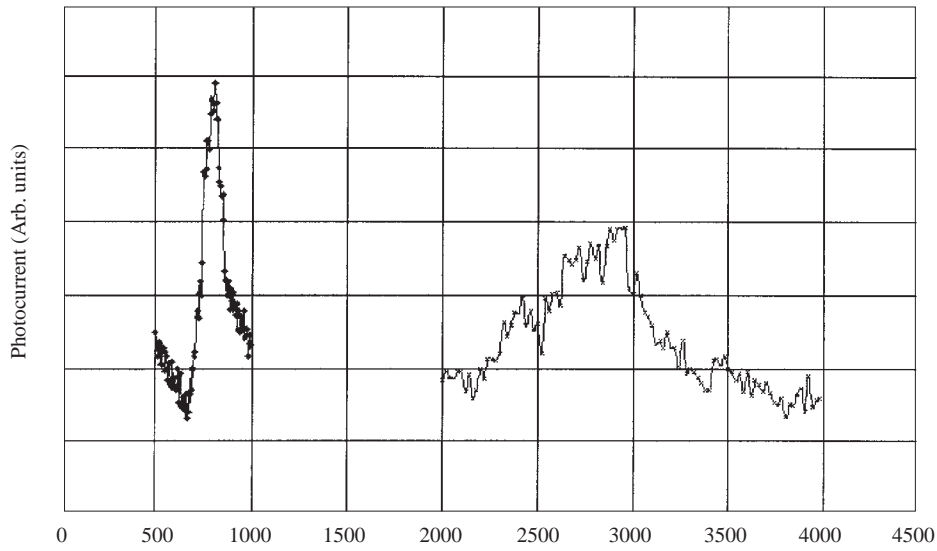


**Figure 2.** Measured photo-current for sample 1262 at 78K showing the interband transition (700-900 nm) and intersubband transition (2.3-3.3  $\mu\text{m}$ ).

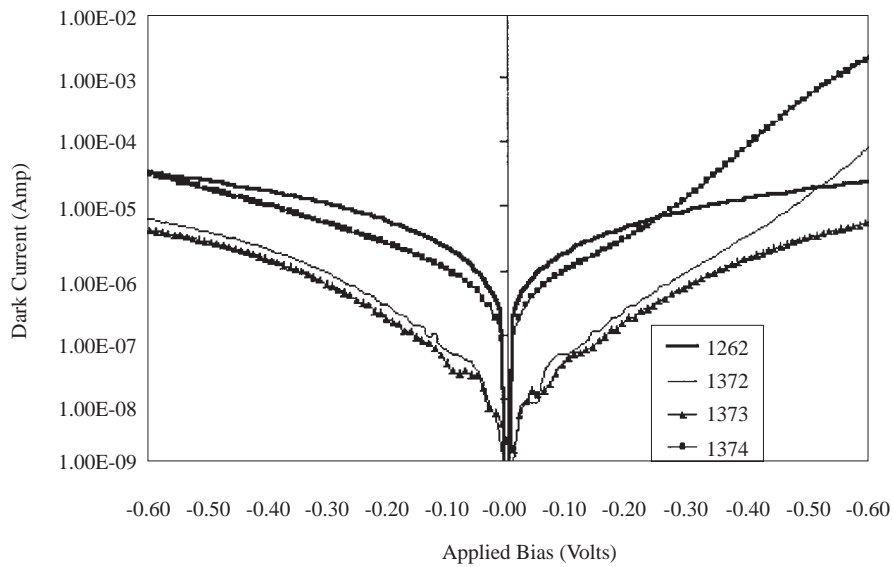


**Figure 3.** Dark current for 400 mm diameter devices measured at 150K.

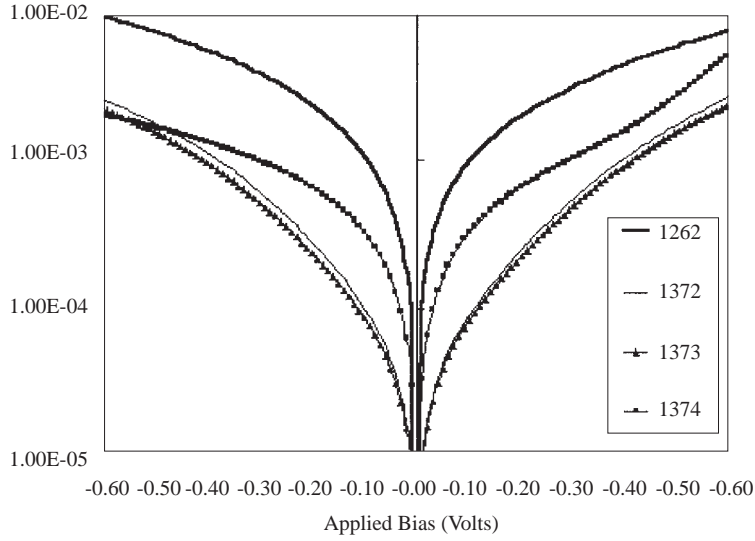


**Figure 4.** Dark current for 400  $\mu\text{m}$  diameter devices measured at 230K.

The voltage-dependent dark current may be calculated from

$$I_d = eAv_d n \quad (1a)$$

$$= e \frac{Av_d}{L_p} \int T(E, V) f(E) \rho(E) dE \quad (1b)$$

where  $f(E)$  is the Fermi factor,  $\rho(E)$  is the 2D electron density of states,  $L_p = a_1 + a_2 + c + b_1 + b_2$  is the period of the MQW structure,  $v_d$  is the drift velocity, and,  $T(E, V)$  is the voltage-dependent transmission coefficient. For a QWIP structure dark current normally has three components: thermionic emission, thermally-assisted tunnelling and temperature-independent tunnelling. Large separation between the wells ( $\sim 300\text{-}500\text{\AA}$ ) implies that the last contribution to dark current is negligible. For thermionic emission the transmission coefficient  $T=1$  for energy  $E > V_B$ , where  $V_B$  is the height of the barrier. Thermally-assisted tunnelling is the tunnelling of thermally excited electrons through a triangular barrier in an applied electric field, and the transmission co-efficient, in the WKB approximation, is

$$T_{th-t} = \exp \left[ -\frac{4}{3eV_1} \sqrt{\frac{m_B^* L_B^2}{2\pi^2 \hbar^2}} (V_B - E)^{1.5} - (V_B - E - V_1)^{1.5} \right] \quad (2)$$

where  $V_1$  is the voltage drop across one period of the MQW and  $m_B^*$  is the electron effective mass in the barrier. For the resonant tunnelling QWIPs under study here we have considered an additional contribution to the dark current: thermally-assisted resonant

tunnelling current. The presence of high AlAs double barriers modifies the density of states for  $E \sim E_2$ , where  $E_2$  is the energy of the first excited level. This contribution to the dark current may be important at high temperatures/voltages.

At 150K (Fig. 3) the samples 1262 and 1374 exhibit similar voltage-dependence and order of magnitude of the dark current. The same is seen for samples 1372 and 1373. However, 1372 and 1373 show dark currents an order of magnitude smaller than those for 1262 and 1374. It is seen from the Table that 1372 and 1373 have 40% aluminum in the lower (thicker) AlGaAs barrier while 1262 and 1374 have only 32% Al. Therefore, the experimental results of figure 3 may be understood in terms of thermionic emission over the AlGaAs barrier being the dominant mechanism for dark current at this temperature. Calculation of dark current using Eqs. (1) and (2) shows that the contribution from the thermally-assisted tunnelling is almost negligible and the experimentally measured temperature dependence of the dark current can be modelled by thermionic emission of electrons over a potential barrier  $V_B$ , where,  $V_B \simeq 480\text{meV}$  for 1262 and 1374 and  $V_B \simeq 540\text{meV}$  for 1372 and 1373. These values of  $V_B$  are close to the energy band offset between  $\text{In}_{0.22}\text{Ga}_{0.78}\text{As}$  and the  $\text{Al}_x\text{Ga}_{1-x}\text{As}$  barrier. The high, thin AlAs barriers appear to be almost transparent [6], though the dark current for 1373 is lower than for 1372 which has thinner AlAs barriers. Sample 1374 shows a similar trend compared to 1262.

At the higher temperature of 230K (figure 4) the dark currents for 1372 and 1373 still follow a trend similar to each other (although the currents for all samples are orders of magnitude larger). Samples 1262 and 1374, on the other hand, exhibit dark current magnitude and profiles which are different from each other. The high-voltage dark current for 1374 is much closer to that for 1372 and 1373. This may indicate the presence of the resonant tunnelling contribution mentioned above.

### Concluding remarks

A QWIP operating at  $\sim 3$  mm with a normal-incidence component has been demonstrated and its dark current characteristics were studied in some detail. The collector efficiency of this device is expected to be good since the electrons are photo-excited into a resonant tunnelling energy state. The measured dark current is too large to be explained by thermionic emission over the AlAs barriers and appears to be dominated by thermionic emission over the lower (thicker) AlGaAs barriers. Therefore, it has been possible to improve the dark-current characteristics of the device by increasing the Al concentration in the AlGaAs barriers (figs. 3 and 4). Work is in progress on other samples with a view to optimising the dark current for these structures.

### Acknowledgments

This work is supported by EPSRC (ROPA project). We are grateful to Dr. Bob Grey (Sheffield University) for growing the samples and to Dr. Geoff Hill for processing them.

**References**

- [1] Levine, B. F., J. Appl. Phys. 74 (1993) R1. Also see references therein.
- [2] Ed. Mannasreh, M. O., Semiconductor Quantum Wells and Superlattices for Long-Wavelength Infrared Detectors.(Artech House, London) 1993.
- [3] Liu, H. C. Buchanan, M. and Wasilewski, Z. R., J. Appl. Phys. 83 (1998) 6178.
- [4] Liu, H. C. Buchanan, M. and Wasilewski, Z. R., Appl. Phys. Lett. 72 (1998) 1682.
- [5] Whitney, R. L. Cuff, K. F. and Adams, F. W., Reference 2, p.55.
- [6] Landheer, D. Liu, H. C. Buchanan, M. and Stomer, R., Appl. Phys. Lett. 54 (1989) 1784.